Angular emission of ions and mass deposition from femtosecond and nanosecond laser-produced plasmas

B. Verhoff, S. S. Harilal, and A. Hassanein
Center for Materials Under Extreme Environment, School of Nuclear Engineering, Purdue University, West Lafayette, Indiana 47907, USA

(Received 28 March 2012; accepted 22 May 2012; published online 25 June 2012)

We investigated the angular distribution of ions and atoms emanating from femto- and nanosecond laser-produced metal plasmas under similar laser fluence conditions. For producing plasmas, aluminum targets are ablated in vacuum employing pulses from a Ti:Sapphire ultrafast laser (40 fs, 800 nm) and an Nd:YAG laser (6 ns, 1064 nm). The angular distribution of ion emission as well as the kinetic energy distribution is characterized by a Faraday cup, while a quartz microbalance is used for evaluating deposited mass. The ion and deposited mass features showed that fs laser ablated plasmas produced higher kinetic energy and more mass per pulse than ns plumes over all angles. The ion flux and kinetic energy studies show fs laser plasmas produce narrower angular distribution while ns laser plasmas provide narrower energy distribution. © *2012 American Institute of Physics*. [http://dx.doi.org/10.1063/1.4730444]

I. INTRODUCTION

Laser-produced plasmas (LPP), formed when a high power laser focused on a target, have been the focus of numerous fundamental studies since the discovery of lasers in 1960s. Currently, there exist extensive industrial and defence applications of LPP, and the majority of these plasmas are generated by nanosecond pulses.[1] However, with the invention of chirped pulsed amplification (CPA) method in 1990s, which stretches the laser pulse in time prior to amplification, and the discovery of high fluence solid state materials like Ti-Sapphire lead to revolutionary development in the peak power of table-top lasers. Since then fs lasers have been explored for use in many promising applications, e.g., micromachining,[2] laser surgery,[3] surface smoothing,[4] nanoparticle production,[5] generation of collimated proton,[6] electron, neutron beam,[7] etc. LPP also produce high intensity ion beams with various charge states.[8] Moreover, the properties of laser plasma ions (charge state, flux, etc.) change with angle with respect to target normal and depend strongly on the irradiation conditions (laser and target properties, angle of incidence, etc.). This can limit its ability to be applied to different applications and therefore requires further studies to improve the dynamics of ion emissions from LPP.

Directed laser energy impact on any matter leads to heating and consequent plasma formation. However, the laser-matter and laser-plasma interaction properties as well as the behavior of subsequently generated plasmas vary widely with the excitation source pulse width as well as wavelength. The femtosecond laser light is absorbed most efficiently by the material surface and the lifetime of the laser pulse is usually too short that there is no significant interaction between the laser pulse and plasma. In nanosecond LPP, the leading edge of the laser interacts with the target surface, and the rest of the laser energy is imparted to the expanding plasma for further reheating. It should be noted that the fs pulses have significantly lower laser ablation (LA) threshold fluence compared to ns laser ablation threshold fluence, and hence, shorter pulses produce significant plasma intensity at lower laser fluence levels.[9] According to Ref. 9, the threshold fluence for ablation is more or less constant when the pulse width of the laser is <100 ps while the threshold laser fluence increases with pulse duration when it is >100 ps. The heat affected zone (HAZ) observed for ns laser ablation (nLA) is typically 100 μm to 1 mm, whereas very small HAZ is noticed for fs laser ablation (fLA) due to very limited penetration length of thermal diffusion.[10] In fs laser-target interaction, the electron to ion energy transfer time (τ_{ei}) and heat conduction time (t_{heat}) exceeds the duration of the excitation laser pulse ($\tau_{ei} \sim t_{heat} \gg t_p$). By focusing femtosecond lasers, high intensity in the range of 10^{14} W/cm^2 or higher is possible. This laser intensity generates extremely high electric and magnetic fields at the target surface, and the produced plasma emits high energy, bright emission of electrons, and x-rays.[11,12] Because of efficient laser-plasma heating, the nanosecond LPP provide efficient sources in the EUV spectral region.[13]

Recent studies showed that fs LPP have two plumes, an atomic and nanoparticle plume but for nanosecond plume, only the atomic plume is commonly seen in earlier times.[14] In nanosecond LPP, the spread of ions was found to have broader profile than the fs LPP.[5,15] Currently, ultrashort pulses are actively considered for many LA applications previously used with ns "long pulse" lasers, which includes LA sample introduction in inductively coupled plasma mass spectrometry (ICP-MS), laser-induced breakdown spectroscopy (LIBS), pulsed laser deposition (PLD), micromachining, etc., because of certain advantages. For example, it was shown that fs laser ablation sample introduction in the ICP-MS provides uniform aerosol size distribution which reduces elemental fractionation.[16] Recent reports showed that ultrafast PLD minimizes the formation of droplet which is often seen with ns PLD.[17] The fs LIBS is found to provide lower continuum compared to traditional ns LIBS.[18]

Understanding the angular and energy distribution of atoms and ions in ns and fs, LPP is very important for optimizing their parameters and conditions for various applications. In this paper, we report on the dynamics of ion emission and mass deposition from ns and fs laser ablated plasmas from aluminum targets in vacuum under similar laser fluence conditions. Though similar laser fluence conditions are used for the present studies for ns LPP and fs LPP, it should be noted that the power densities used are differed by more than 5 orders in magnitude.

II. EXPERIMENTAL SETUP

The schematic of the experimental set up used in the present investigation is shown in Fig. 1. The Nd:YAG ns laser (Surelite I, Continuum lasers) provides 10 Hz, 6 ns FWHM pulses at a wavelength of 1064 nm. A combination of wave plate and polarizing cube was used for attenuating the energy of the ns pulse. The fs laser consists of mode-locked Ti-Sapphire oscillator (Synergy 20, Femtolasers), which gives <35 fs pulses at 800 nm. The amplifier system (Amplitude Technologies, Model Pulsar) consists of stretcher, regenerative amplifier, multi-pass amplifier, and a compressor providing 10 Hz, 40 fs pulses with maximum energies ~10 mJ. The energy of the fs laser output is varied using a polarizer positioned before the compressor gratings. For producing plasmas, an Al target was positioned in a evacuated chamber with base pressure $\sim 10^{-5}$ Torr. The target is moved using an externally controlled xyz translator for providing fresh surface. The p-polarized laser beam is focused onto the target using plano convex lens at 45° angle of incident with respect to target normal. The approximate spot size at the target surface was $1 \times 10^3\ \mu m^2$ at a laser energy of 6 mJ.

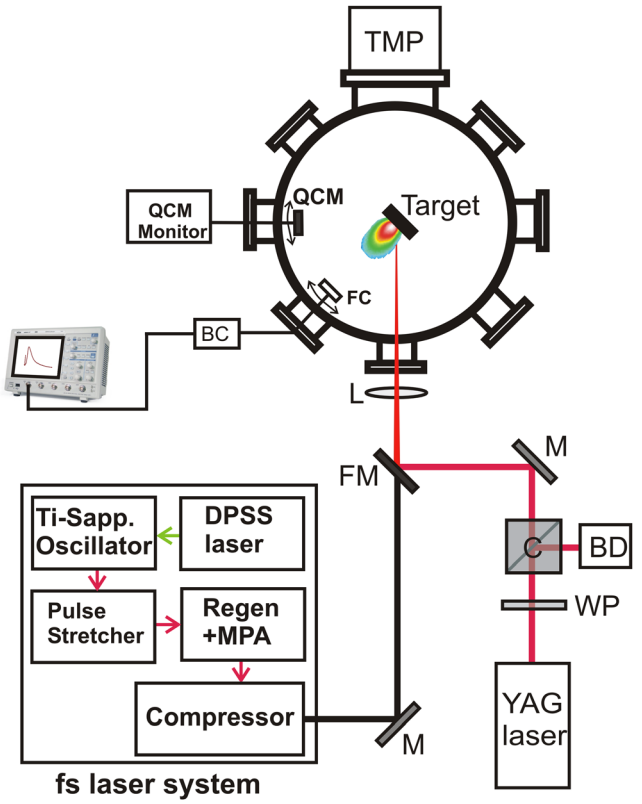

FIG. 1. Schematic of the experimental set up. The target is positioned in a evacuated chamber at 10^{-5} Torr. (QCM—Quartz crystal microbalance, FC—Faraday cup, BC—biasing circuit, TMP—turbomolecular pump, L—Lens, FM—flip mirror, M—mirror, BD—beam dump, WP—wave plate).

The plasma diagnostic tools used include a Faraday cup (FC) and a quartz crystal microbalance (QCM). The FC was positioned 14 cm away from the target and a vacuum manipulator allowed the FC to be rotated through off-normal target angles between 0° and 65° with high angular precision. The FC consisted of an input aperture 2 mm and biased at −31 V to screen off the electrons. The QCM was placed on the same manipulator and was positioned 12 cm from the target with a 0.5 mm^2 area allowing for the angular dependency studies. The QCM consists of silver-coated crystal microbalance sensor attached to an Inficon XTM-2 deposition monitor. Unlike FC, the QCM crystals are less sensitive to deposited mass and requires several hundred pulses for obtaining measurable deposition rate on the crystals. Hence, the ion profiles are obtained with single shot laser ablation, while 600 pulses were used for estimating mass deposition rate.

III. RESULTS AND DISCUSSION

Understanding the ion emission features from laser ablation plumes is important for many of its applications. We utilized the FC for measuring kinetic distributions of Al ions. Faraday cups are routinely used for charge analysis in laser-produced plasmas. However, it should be noted that space charge effects could distort the FC signal.[19] Other limitations that can occur using a FC arise from the ability to determine the exact charge state of the ion being collected because it works strictly of the number of charged ions. Nevertheless, FC provides useful information of the total ion flux as well as maximum probable kinetic energy for ions emanating from the plume. Depending on charge state, ions can possess different kinetic energies due to space-charge effects. The typical time of flight (TOF) profiles recorded are given in Fig. 2 for both ns and fs LPPs and for various angles with respect to target normal. The laser incident angle is 45° with respect to target surface and similar laser energy density was used for both ns and fs laser excitations. The ns ion signal has a delayed start time compared to the fs ion flux, indicating the difference in their velocities.

The ion kinetic profiles show that the ions emanating from fs plasmas have higher kinetic energies irrespective of angle of observation with respect to target normal. Plasma and ion formation mechanisms in ns and fs plasmas are different due to the time needed for the laser to interact with target lattice atoms. Generally, the electron-lattice relaxation time in metals is 1–10 ps. Thermal ablation occurs when the pulse width of the laser is longer than the electron-lattice relaxation time. Hence, for ns laser ablation, the process of laser-target interaction is thermodynamic where the plasma is generated by evaporation of the heated material.[20] After the generation of the plasma, the rest of the laser beam is used to heat the plasma instead of contacting the target material.[21] The fs laser interaction does not rely on such interaction because the laser

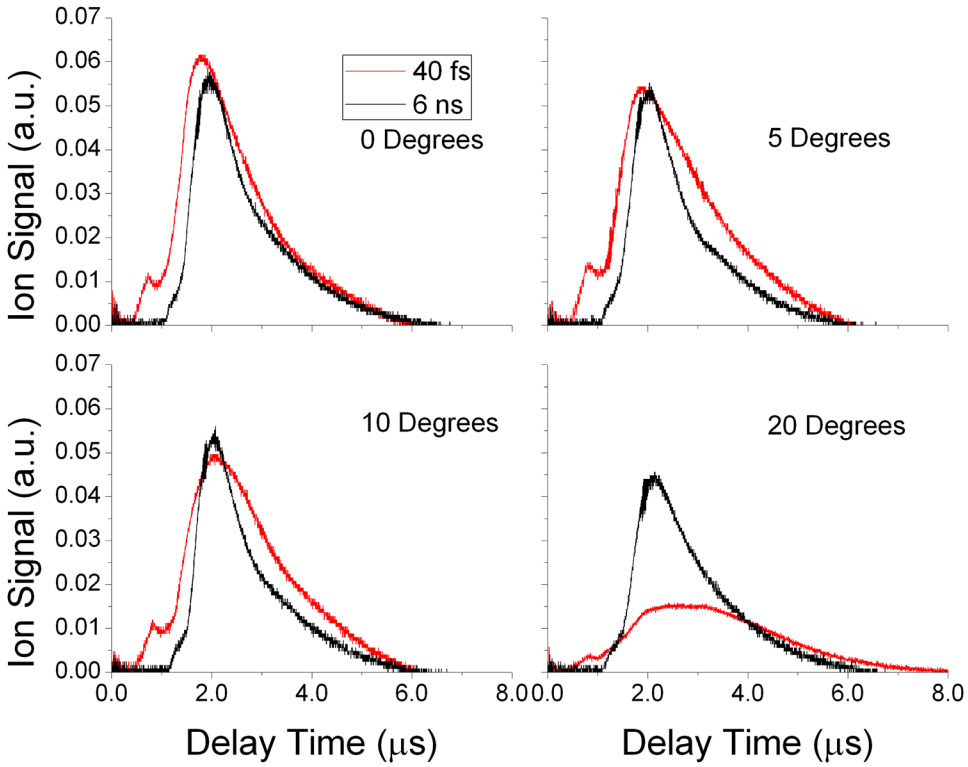

FIG. 2. Ion flux profiles at different angles of 0°, 5°, 10°, and 20° off target normal using similar energy fluence with 40 fs 800 nm laser (red) and 6 ns 1064 nm laser (black). The laser angle of incidence is 45° and the ion flux profile was measured using faraday cup located 14 cm from target surface, at a laser energy of 6.5 mJ.

deposits the entire energy to the electrons directly before any plasma formation.[22] When the laser pulse width is shorter than the electron-phonon relaxation time, the electrons proceed to higher temperatures while the lattice remains cold, and hence, the conventional hydrodynamics motion does not occur during the fs interaction time.

A distinct feature noticed with fs laser ablation is the observation of a faster kinetic energy peak in the ion TOF profiles. The faster peak seen in the ion temporal profiles of fs LPP has been reported previously by several groups.[23–25] Recently, Donnelly *et al.*,[7] observed a dual peak structure in their ion profiles recorded using a planar Langmuir probe during 250 fs laser ablation of Ni at a laser fluence of 0.6 J/cm^2 and assigned the faster kinetic energy peak to low-Z contamination of the target surface. To verify the observation of dual peak ion structure in the present experiment is simply due to low-Z contaminant, multiple laser shots were fired at the same target position. We have seen the dual peak structure in the ion profiles even after 300 shots at the same target position and the reduction in the ion intensity of the faster peak is found to be relative to the slower hydrodynamic component, and hence, we believe that the observation of faster ion component in the present experiment is not due to target contamination. Zhang *et al.*[26] noticed two distinct ion population during ultrafast laser ablation of Al and described as the accelerated component originated from a combination of ambipolar field effects, Coulomb explosion, nonlinear pondermotive effects. Amoruso and co-workers[27] reported double peak distribution of electron and ion emission profile during TOF mass spectroscopic measurement during fs ablation of Cu and Au and explained this due to space-charge effect. Similar double peak ion distribution is also noted at higher intensity ultrafast ablation ($\sim 10^{15}$ Wcm^{-2}) of carbon target and explained due to ion acceleration caused by rapid formation and expansion of a space-charge layer of electrons, which creates a time-dependent ambipolar field.[27,28] Ye and Grigoropoulos[29] varied the fluence and measured the time of flight profile from a titanium target stating that the first sharp peak was made of singly charged titanium.

In fs laser ablation, the absorbed laser energy is deposed as electron thermal energy while the ions remains cold inhibiting conventional thermal expansion. However, if the laser intensity is high enough, the electrons can gain energy in excess of the Fermi energy and escape from the target. The escaped electrons accelerate the ions by the electrostatic field of charge separation. According to Gamaly *et al.*[30] this regime occurs at the laser pulse duration of $t_p < 200$ fs and at laser power densities $>10^{14}$ W/cm^2. The power density used in the present studies is $>10^{14}$ W/cm^2, and hence, we believe that the observation of faster peak in the ion kinetic energy profiles is due to space-charge effect. The space charge effect can accelerate ions to higher energies in a plasma prior to the lower energy ions seen in the second peak, which is similar to the hydrodynamic component observed in ns LPP.

The ion energy profiles can be derived from the ion TOF spectrum and are shown in Fig. 3 for various angles with respect to the target normal. The maximum probable energy of the ions produced from both ns and fs plasma decrease with an increase in off-normal angles. Narrower kinetic energy (KE) profiles are obtained for ns LPP where the maximum probable KE is ~500–1000 eV. The kinetic energy ion distributions of ns LPP can usually be described by a shifted Maxwell-Boltzmann (SMB) distribution.[31] However, the recorded KE profiles are broader for fs ions and can be represented by a two-peak structure. The fast kinetic energy peak, KE is ~3000–4800 eV, is more evident at near normal

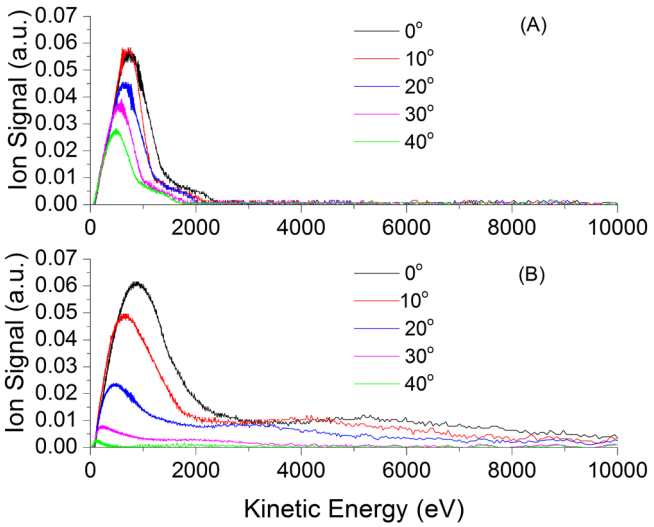

FIG. 3. Kinetic energy profiles at different angles from off target normal with similar energy fluence at an angle of incidence of 45° in vacuum at 10^{-5} Torr and a laser energy of 6.5 mJ for (A) 6 ns pulse at 1064 nm (B) 40 fs pulse at 800 nm.

angles and significantly broader than the observed slow KE profile with maximum ion kinetic energy spread exceeding 10 keV.

The estimated maximum probable KEs and ion flux from TOF profiles of ns and fs LPPs are shown in Fig. 4.

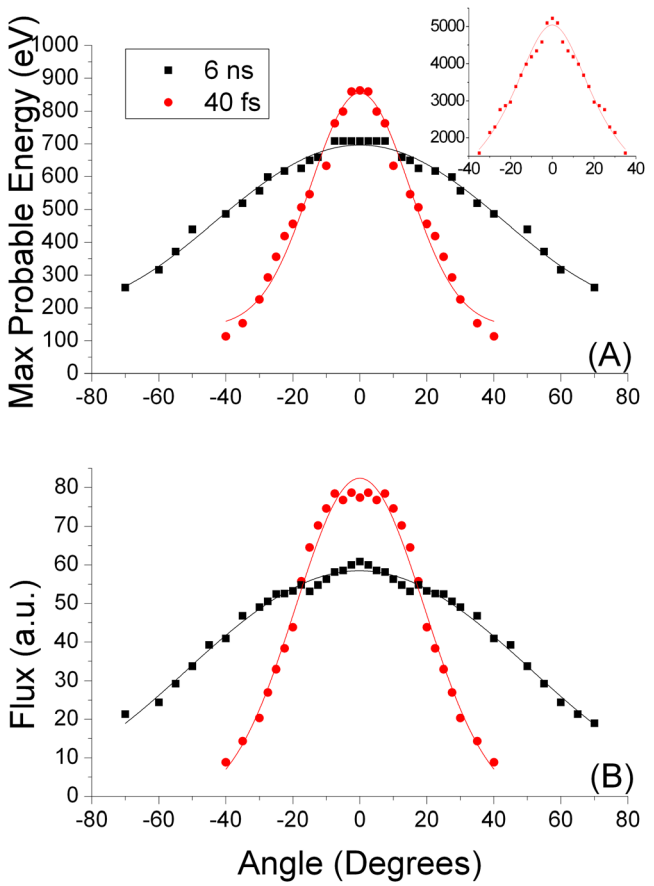

FIG. 4. FC data measured at 14 cm from Al target at incident of 45° off normal for ns and fs lasers, at an energy of 6.5 mJ. (a) Maximum probable energy with respect to angle. The inset in figure corresponds to observed faster kinetic peak in fs plume. (b) Total ion flux vs angles off target normal for 6 ns 1064 nm pulse and 40 fs 800 nm.

Measurements were made for only positive angles but copied to their negative angles for comparison assuming hemispherical expansion of the plume. Compared to ns LPP ions, the fs LPP ions have higher maximum probable kinetic energy between ±15° with respect to the target normal. The maximum probable energy from the fs laser has 74% decreases from 0° to 30° off normal whereas the ns laser has a decrease of 22%. This indicates most of the ions ejected by the fs LPP contained in narrow cone angle with respect to the target normal. For the ns laser, a larger number of ions are emitted around the outer edges of the sphere increasing its cone angle. The estimated ion emission cone angle with respect to target normal for fs plasma is 17° ± 1°, while it is 45° ± 2° for ns plume. The estimated cone angle for the high-energy ion peak in fs LPP matches the lower energy cone angle (seen in Fig. 4(a) inset).The broadening of the ion distribution in the ns plume is attributed to the recombination of the higher charged ions.[32,33] Previous studies[34] used Gaussian widths for measuring angular distribution of ion particles and noticed decreasing width with increasing ion mass and ionization for ns produced plasmas. The solid lines given in Fig. 4 correspond to a Gaussian fit and the ion flux FWHM is 38.5 and 106 for fs and ns LPP, respectively. The estimated ion flux FWHM is a factor of ∼3 lower for fs LPP compared to ns LPP. The preferential ion expansion of fs LPP in the normal direction can be understood by considering the pressure confinement due to strong overheating in the laser impact zone. Since the entire energy is deposited on the target electrons before electron-lattice energy transfer or plasma formation, higher temperature can be expected in fs laser plasmas, leading to high pressure zone in the laser impact zone.

We also analyzed the distribution of mass deposited at various angles with respect to target normal using QCM. Figure 5 shows the recorded deposit of mass per pulse for ns and fs laser ablation. Since the deposited mass per pulse is ∼ pg, each data point is obtained by averaging over 600 pulses. Using a QCM to determine the mass of the ejected atoms from the surface allows more accurate description of angular dependence. The FC results showed the ion flux from the plume; however, the QCM data is not necessary

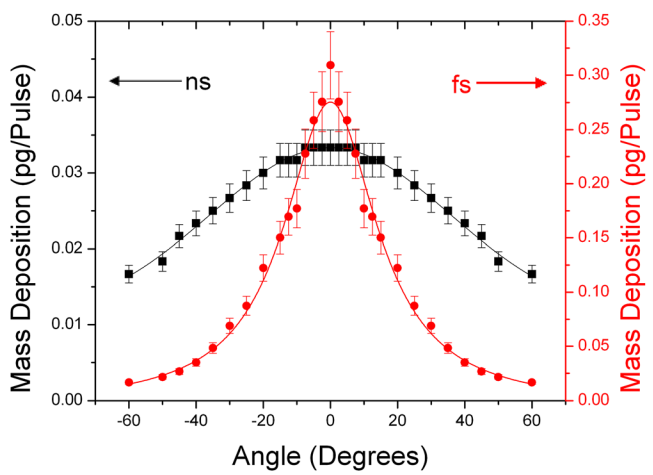

FIG. 5. Mass deposition per pulse vs angle off target normal on QCM crystal positioned 12 cm away from the target at a laser energy of 6.5 mJ with laser pulse of 40 fs 800 nm and 6 ns 1064 nm.

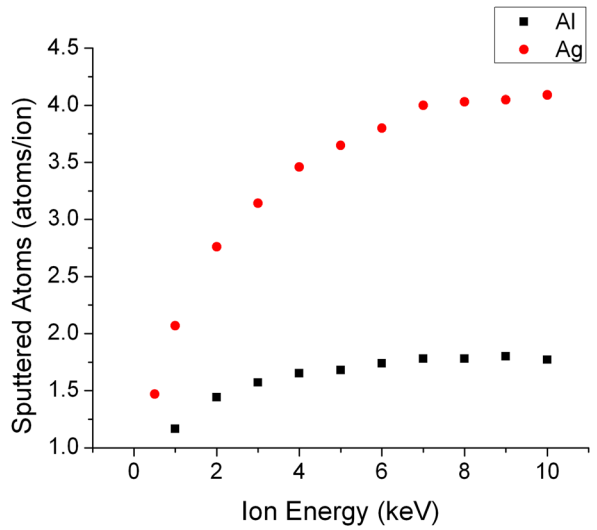

FIG. 6. Sputtered atoms vs ion energy dependence using ITMC code to simulate interaction on the QCM surface.

totally due to atomic deposition. The deposited mass can contain both ions and neutrals. Moreover, the energetic ions can sputter off the deposited mass. Therefore, if the energetic ions are interacting with deposited particles on the QCM and the QCM crystal itself, the ions can sputter off the deposition lowering the total mass deposition.

We estimated the amount of sputtered atoms by the energetic ions using Ion Transport in Materials and Compounds (ITMC) code.[35] The deposited Al atoms can be sputtered from the QCM crystal by energetic ions emanating from laser-plasma along with sputtering of the QCM crystal material (Ag) itself. The ITMC calculations, shown in Fig. 6, give the number of sputtered atoms per ion at energies between 0.5 and 10 keV corresponding to the most likely ions produced from the fs laser produced plasma. Along with the estimation of number of sputtered Al atoms/ion, sputtering yield for silver is also included in the Fig. 6 because the QCM crystal having Ag coating. The sputtering ratio for silver is approximately 3 times larger than that of the aluminum, but assuming aluminum coats the crystal during ablation, the ions have a higher probability of sputtering off aluminum compared to silver indicating little deviation from expected deposition due to its lower sputtering ratio. The higher energetic ions do have higher sputtering yield; however, according to Fig. 3, the higher energy ion flux is significantly lower, therefore less ions are available for sputtering.

The angular distribution of the deposited mass showed significantly different profiles for ns and fs laser plumes. The difference in mass ablated between the ns and fs in Fig. 5, was on the order of 15 times larger for the fs laser compared to the ns laser at low angles. This difference in deposited mass measurements becomes less at larger angles. In ns laser plasmas, a part of the energy is used for sample heating and phase transition into the gasous state and the rest of the laser energy is used for reheating the ablated species. In the case of fs laser plasma, no ablated material is expected above the target surface until the end of the laser pulse. This scenario makes significantly higher ablation efficiency for fs laser plasmas than with longer pulses where laser pulse energy is partly screened by ablated materials. Hence more effective ablation can be expected from fs LPP due to laser energy confinement leading to forward expansion of ablated particles.[17] The fs LPP deposits mass heavily for angles within 20° off target normal while the ns LPP continues to provide a larger distribution of atoms about the target.[5,15] The solid lines in the Figure 5 represent the best fit curve of the mass ablated for the fs and ns laser interactions with a calculated error of the QCM measurement to be 10%. The Gaussian distribution of the ns LPP coincides with the same distribution

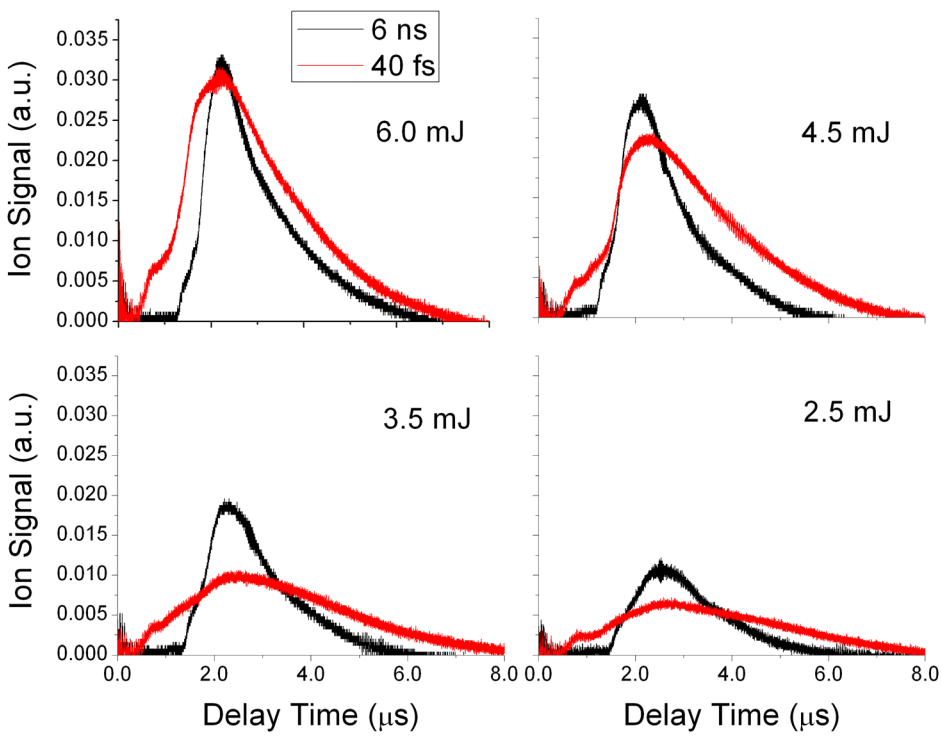

FIG. 7. Ion flux vs delay time for different laser energy of 6.0 mJ, 4.5 mJ, 3.5 mJ, and 2.5 mJ using Faraday cup located 14 cm from Al target at an angle of 10° in 10^{-5} Torr.

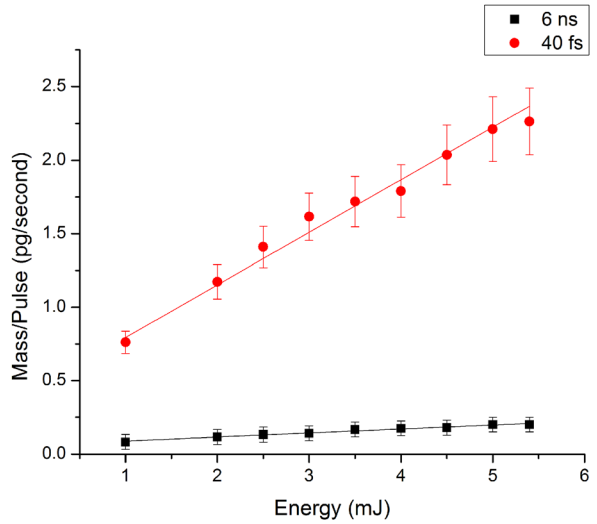

FIG. 8. Dependence of ablated mass on laser energy for fs and ns lasers.

used to analyze the ion dynamics, indicating similar angular emission from ion and atomic debris.[34]

We proceeded to investigate the energy dependence to determine if there is a discernible difference in ion and deposited mass dynamics with changes in laser energy. The TOF profiles obtained for ns and fs laser plumes recorded at 10° with respect to target normal is shown in Fig. 7 for a range of laser energies. The total flux of both ns and fs LPP decreases with decreasing laser energy. The decrease in total ion flux vs laser energy was measured and the fs laser has a slope of about 9.8 while the slope for the ns laser is about 6.2. Hence, the reduction in total ion flux for fs LPP is more rapid compared to ns LPP. This can be understood considering the difference in laser-target coupling in fs and ns laser ablation. The laser target coupling for the ultrashort laser pulse imparts the entire energy of the pulse with the target material and the ion flux changes proportionally with laser input energy. However, in the case of the ns LPP, the increased energy is mainly used for reheating the expanding plasma rather than interacting with the target.

The variation of the mass deposition rate with respect to laser energy for ns and fs LPP is given in Fig. 8. For this measurement, the QCM was positioned at 10° with respect to the target normal. The deposited mass follows a linear increasing trend for both LPP with increasing laser energy. However, at any particular energy studied the amount of fs mass deposition is higher compared to the ns LPP mass deposition. The linear fitting given in Fig. 8 (solid lines) show that the fs and ns LPP follow a slope of 0.35 and 0.03 pg/(mJ*s) respectively, indicating mass ablation rate enhances rapidly with increasing laser energy for fs compared to ns LPP. This large increase in fs laser ablation follows the same interaction mechanisms seen in ion total flux calculations that are associated with efficient laser-target coupling. The ns laser energy has little impact on the variation of mass deposition in the small energy range used.

IV. CONCLUSIONS

We investigated the angular distribution of ions and ablated mass of femtosecond and nanosecond laser-produced metal plasmas. For systematic comparison, we maintained similar laser fluence levels for both ns and fs plasmas, though the laser power densities at the target surface differ by 5 orders of magnitude. The ion emission was characterized using Faraday cup, while a quartz microbalance was used for measuring the deposited mass. The ion flux and kinetic energy studies of the fs laser plasmas show narrower angular distribution while ns laser plasmas provide narrower energy distribution. The kinetic ion profiles of fs LPP showed a faster broad kinetic peak followed by a slower peak. The ns LPP ion profiles showed only a single peak structure. The observation of faster kinetic energy peak in the fs laser plumes is explained due to space charge effect which can accelerate ions to higher energies in plasma prior to the lower energy ions seen in the second peak which is similar to the hydrodynamic component observed in ns LPP. In addition, the maximum probable kinetic energies (slower peak) of the fs LPP is higher at short angles from target normal compared to ns LPP.

The deposited mass studies at similar laser fluence levels showed fs laser mass ablation to be significantly higher compared to ns laser. Angular dependence of mass deposition profiles showed forward biasing for fs plume compared to the ns plume. The peak deposited mass is nearly 15× higher for fs LPP compared to ns LPP for the parameters used in our study. This can be understood because of the differences in laser-target coupling. For fs the laser energy is mainly deposited on the target and hence ablation efficiency will be higher, while for ns laser, large part of the laser energy is deposited within the expanding plasma for reheating the ablated materials.

The laser energy dependence on ion emission showed the increase in ion flux to be more rapid for fs compared to ns LPP for the range of laser energies studied. However, it should be mentioned that the changes in ion flux depends strongly on angle of observation. Narrower ion kinetic profiles are also observed with increasing laser energy for both ns and fs LPP. The dependence of the deposited mass on laser energy showed significant difference from ion flux variation with laser energy. The deposited mass increases rapidly with increasing laser energy for fs LPP. The slope of the fs LPP was an order of magnitude larger than the ns LPP indicating much higher ablated material for fs laser.

ACKNOWLEDGMENTS

The authors thank Tatyana Sizyuk for the ITMC calculations and Al-Montaser Al-Ajlony for the initial experimental help. This work was partially supported by the U.S. DOE, office of National Nuclear Security Administration under Award number DE-NA0000463.

[1]J. F. Ready, *Industrial Applications of Lasers*, 2nd ed. (Academic Press, San Diego, 1997).
[2]G. Cerullo, R. Osellame, S. Taccheo, M. Marangoni, D. Polli, R. Ramponi, P. Laporta, and S. De Silvestri, Opt. Lett. **27**, 1938 (2002).
[3]R. M. Kurtz, J. A. Squier, V. M. Elner, D. Du, X. B. Liu, A. Sugar, and G. A. Mourou, Investigative Ophthalmology & Visual Sci. **35**, 1786 (1994).
[4]N. H. Rizvi, RIKEN Rev. **50**, 107 (2003).
[5]S. Amoruso, T. Donnelly, J. G. Lunney, R. Bruzzese, X. Wang, and X. Ni, Appl. Phys. A **100**, 569 (2010).
[6]B. X. Hou, J. Nees, J. Easter, J. Davis, G. Petrov, A. Thomas, and K. Krushelnick, Appl. Phys. Lett. **95**, 101503 (2009).

[7]T. Donnelly, J. G. Lunney, S. Amoruso, R. Bruzzese, X. Wang, and X. Ni, J. Appl. Phys. **108**, 043309 (2010).
[8]J. Badziak, A. A. Kozlov, J. Makowski, P. Parys, L. Ryc, J. Wolowski, E. Woryna, and A. B. Vankov, Laser Particle Beams **17**, 323 (1999).
[9]E. G. Gamaly, A. V. Rode, B. Luther-Davies, and V. T. Tikhonchuk, Phys. Plasmas **9**, 949 (2002).
[10]Y. Hirayama and M. Obara, J. Appl. Phys. **97**, 064903 (2005).
[11]R. C. Issac, G. Vieux, B. Ersfeld, E. Brunetti, S. P. Jamison, J. Gallacher, D. Clark, and D. A. Jaroszynski, Phys. Plasmas **11**, 3491 (2004).
[12]K. Krushelnick, E. L. Clark, R. Allott, F. N. Beg, C. N. Danson, A. Machacek, V. Malka, Z. Najmudin, D. Neely, P. A. Norreys, M. R. Salvati, M. I. K. Santala, M. Tatarakis, I. Watts, M. Zepf, and A. E. Dangor, IEEE Trans. Plasma Sci. **28**, 1184 (2000).
[13]A. Hassanein, T. Sizyuk, V. Sizyuk, and S. S. Harilal, J. Micro/Nanolith. MEMS MOEMS **10**, 033002 (2011).
[14]M. E. Povarnitsyn, T. E. Itina, M. Sentis, K. V. Khishchenko, and P. R. Levashov, Phys. Rev. B **75**, 235414 (2007).
[15]A. H. Dogar, B. Ilyas, H. Qayyum, S. Ullah, and A. Qayyum, Eur. Phys. J. Appl. Phys. **54**, 10301 (2011).
[16]J. Koch, A. von Bohlen, R. Hergenroder, and K. Niemax, J. Anal. Atomic Spectr. **19**, 267 (2004).
[17]S. Canulescu, E. Papadopoulou, D. Anglos, T. Lippert, M. J. Montenegro, S. Georgiou, M. Dobeli, and A. Wokaun, Appl. Phys. A **105**, 167 (2011).
[18]S. Yalcin, Y. Y. Tsui, and R. Fedosejevs, J. Anal. Atomic Spectr. **19**, 1295 (2004).
[19]R. Janmohamed, G. Redman, and Y. Y. Tsui, IEEE Trans. Plasma Sci. **34**, 455 (2006).
[20]J. Yoo and H. S. Lim, J. Mech. Sci. Technol. **25**, 1811 (2011).
[21]J. J. Chang and B. E. Warner, Appl. Phys. Lett. **69**, 473 (1996).
[22]C. R. Phipps, *Laser Ablation and Its Applications* (Springer, New York, 2007).
[23]G. O. Williams, S. Favre, and G. M. O'Connor, Appl. Phys. Lett. **94**, 101503 (2009).
[24]S. Amoruso, X. Wang, C. Altucci, C. de Lisio, M. Armenante, R. Bruzzese, and R. Velotta, Appl. Phys. Lett. **77**, 3728 (2000).
[25]G. O. Williams, G. M. O'Connor, P. T. Mannion, and T. J. Glynn, Appl. Surf. Sci. **254**, 5921 (2008).
[26]Z. Zhang, P. A. VanRompay, J. A. Nees, and P. P. Pronko, J. Appl. Phys. **92**, 2867 (2002).
[27]S. Amoruso, X. Wang, C. Altucci, C. de Lisio, M. Armenante, R. Bruzzese, N. Spinelli, and R. Velotta, Appl. Surf. Sci. **186**, 358 (2002).
[28]P. A. VanRompay, M. Nantel, and P. P. Pronko, Surf. Coat. Technol. **100**, 496 (1998).
[29]M. Q. Ye and C. P. Grigoropoulos, J. Appl. Phys. **89**, 5183 (2001).
[30]E. G. Gamaly, A. V. Rode, V. T. Tikhonchuk, and B. Luther-Davies, Appl. Surf. Sci. **197**, 699 (2002).
[31]S. S. Harilal, B. O'Shay, Y. Tao, and M. S. Tillack, Appl. Phys. B **86**, 547 (2007).
[32]F. Castano, P. Ecija, J. I. Apinaniz, R. Martinez, F. J. Basterretxea, A. Longarte, C. Redondo, and M. N. S. Rayo, Chem. Phys. Lett. **486**, 60 (2010).
[33]F. Castano, J. I. Apinaniz, B. Sierra, R. Martinez, A. Longarte, and C. Redondo, J. Phys. Chem. C **112**, 16556 (2008).
[34]S. N. Srivastava, K. Rohr, and B. K. Sinha, J. Appl. Phys. **99**, 07330 (2006).
[35]T. Sizyuk and A. Hassanein, J. Nucl. Mater. **404**, 60 (2010).